DELPHI Collaboration

DELPHI 2002-067 CONF 601

10 July, 2002

Measurement of the Electron Structure Function at Z^o peak

Bogdan Muryn

Faculty of Phys. and Nucl. Techniques,

Technical University of Mining and Metallurgy, Cracow, Poland

Wojciech Słominski, Jerzy Szwed

Institute of Computer Science,

Jagellonian University, Cracow, Poland

Abstract

The hadronic part of the Electron Structure Function (ESF) has been measured for the first time using the e^+e^- data at electron scattering energy $\sqrt{s} = 92.5 GeV$. The data analysis is simpler than that of the photon structure function. The ESF data are compared to phenomenological models. The GRVLO and SAS parametrizations follow the data whereas GRVHO and LAC1 do not. It is shown that quasi-real photon virtuality is important. The ESF data can serve as a cross-check of both analyses and help in refining existing parametrizations.

Contributed Paper for ICHEP 2002 (Amsterdam)

1 Introduction

The single tag e^+e^- collisions can be used to determine both the photon [1] and electron [2, 3] hadronic structure functions. The case of the photon is studied both theoretically and experimentally since long [1, 4]. The experimental results on the electron structure function are presented for the first time in this paper.
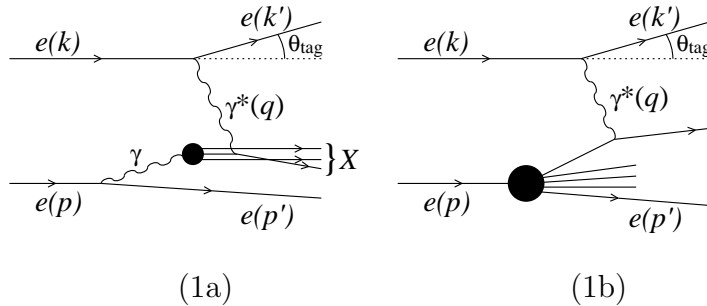

Figure 1: Deep inelastic scattering on a photon target (1a), and on an electron target (1b)

Although both analyses start from the same set of events the procedures are quite different mainly due to different kinematics. In the photon case (Fig. 1a) the spectrum of virtual photons emitted by the (untagged) electron is strongly peaked at small virtualities P^2, so one approximates the photon to be real, however one has to keep in mind that nonzero virtuality plays a role [3]. In the electron case (Fig 1b.) one is dealing with a real particle so the problem does not appear. Another difference is the determination of the Bjorken variable x (for the photon) and z (for the electron). In the first case, since the photon momentum is not known, one is forced to use the total hadronic mass W to determine x,

$$x \cong \frac{Q^2}{Q^2 + W^2} \tag{1}$$

where Q^2 is the negative momentum squared of the deeply virtual (probing) photon. The z variable for the electron is determined simpler - as in the classical deep inelastic scattering i.e. from the deeply scattered electron variables only (see below). A certain drawback of the electron structure function is its expected shape: it contains the sharply peaked photon distribution and is thus dominated by this shape. Having at disposal two methods of analysis it is interesting to compare them and cross-check. We also expect that the data on both the electron and photon structure functions will help to improve phenomenological parametrisations of quark content inside photon and electron.

Let us concentrate on the measurement of the electron structure function. As illustrated in Fig. 1b the upper (tagged) electron emmits a photon of high virtuality $Q^2 = -q^2$ and scatters off the target electron constituents. The cross-section for such process under assumption that $Q^2 \gg P^2$, reads:

$$\frac{d^2\sigma_{ee \to eX}}{dz dQ^2} = \frac{2\pi\alpha^2}{zQ^4} \left[\left(1 + (1-y)^2 \right) F_2^e(z, Q^2) - y^2 F_L^e(z, Q^2) \right], \tag{2}$$

1

where

$$y = 1 - (E_{\text{tag}}/E) \cos^2(\theta_{\text{tag}}/2) \tag{3}$$

with E, E_{tag} and θ_{tag} being the beam electron initial energy, final energy and polar angle, respectively. The parton momentum fraction z is defined in the standard (deep inelastic) way:

$$z = \frac{Q^2}{2pq} = \frac{\sin^2(\theta_{\text{tag}}/2)}{E/E_{\text{tag}} - \cos^2(\theta_{\text{tag}}/2)} \tag{4}$$

and is measured, by means of the tagged electron variables only. The structure function $F_2^e(z, Q^2)$, which dominates the cross-section at small y, has a simple partonic interpretation:

$$F_2^e(z, Q^2) = z \sum_{i=q,\bar{q}} e_i^2 f_i^e(z, Q^2), \tag{5}$$

where e_i and f_i^e are the i-th quark/anti-quark fractional charge and density. In most e^+e^- experiments additional constraints are imposed on the target electron. Since the usual analyses express the same cross-section (2) in terms of the real photon structure functions, one requires this electron to have momentum transfer less than certain value P_{max}^2 ($P_{\text{max}}^2 \ll Q^2$). This procedure leads to "less inclusive" measurement and in practice means that the electron structure functions depend additionally on P_{max}^2.

In a series of papers [2, 3] the construction of the electron structure function has been presented together with the Q^2 evolution equations and their asymptotic solutions. This approach has been also compared with the "photon structure" approach.

Although the determination of the electron and photon structure functions is quite different the functions are simply interrelated:

$$F_2^e(z, Q^2, P_{\text{max}}^2) = \int\limits_z^1 dy_\gamma \int\limits_{P_{\text{min}}^2}^{P_{\text{max}}^2} dP^2 f_\gamma^e(y_\gamma, P^2) \, F_2^\gamma(z/y_\gamma, Q^2, P^2) \tag{6}$$

where the photon flux f_γ^e reads:

$$f_\gamma^e(y_\gamma, P^2) = \frac{\alpha}{2\pi P^2} \left[\frac{1 + (1 - y_\gamma^2)}{y_\gamma} - 2y_\gamma \frac{m_e^2}{P^2} \right] \tag{7}$$

and α is the fine structure constant, m_e — the electron mass and $P_{\text{min}}^2 = m_e^2 y_\gamma^2/(1 - y_\gamma)$.

The above formula means among others that any existing parametrisation of the photon structure function, both real ($P^2 = 0$) and virtual (integrated over P^2), can be tested on the measured electron structure function.

2 Data Selection

A detailed description of the DEPLHI detector and its performance can be found elsewhere [5]. The analysis has been carried out with the data sample collected by DELPHI at the LEP-1 collider during the 1994-1995 annual runs at a centre-of-mass energies ranging from $88.6 GeV$ to $94.6 GeV$ and corresponding to an integrated luminosity of $70 pb^{-1}$.

The essential criterium to select $\gamma\gamma$ events is that one of two scattered electrons [1] was found in the DELPHI luminometer STIC (tag-condition) which covers angular region from

---

[1]electron is used for both - electron and positron.

$43 mrad$ to 166 mrad, whereas the second electron was asssumed to be undetected (antitag condition). Such an event is reffered to as a single-tag event. The energy deposited by tagged electron in the STIC was greater than $0.6 \cdot E_{beam}$ and no additional energy clusters exceeding $0.3 \cdot E_{beam}$ has been detected. The measured energy and an angle of the scattered electron allow to determine transverse squared momentum Q^2.

The further step was to select $\gamma\gamma$ induced hadronic final states - with charged track multiplicity greater than 2. Charged particles were defined as a reconstructed tracks with momenta above $200 \, MeV$, extrapolating to within $4 \, cm$ from the primary vertex in transverse ($R\phi$) plane and within $10 \, cm$ along the beam direction (z-axis). The relative momentum uncertainty for charged particle candidate $\frac{\Delta p}{p}$ had to be smaller than 1, its polar angle with respect to the beam axis was between $20°$ and $160°$ and its measured track length in the TPC was greater than $40 \, cm$. To satisfy the trigger condition at least one of charged tracks had to have momentum larger than $0.7 \, GeV$ and the total energy of all charged tracks was greater than $3 \, GeV$. The minimum of the visible invariant mass of all tracks was fixed at $3 \, GeV$.

In order to supress the Z^0 hadronic background events and τ events the following cuts were implemented:

- The vector sum of the transverse momenta of all charged particles, normalised to total beam energy E_{beam} was greater than 0.12.

- The normalised (like above) sum of absolute values of longitudinal momenta of all particles (including tagged electron) was greater than 0.6.

- The angle between transverse momenta of tagged electron and that of charged particles system had to be greater than $120°$.

- The maximum of the visible invariant mass was $40 \, GeV$.

In order to cut off a background of the off-energy electrons the minimum of the tagged particle energy was increased to $30 \, GeV$.

Among 21 430 events with one high energy deposit in the STIC calorimeter, 2340 events were selected passing the above criteria.

The main background originates from the two-photon production of $\tau\tau$ and their contribution estimated from the simulated data with the same integrated luminosity provided 78 events. The next possible contributions to the background from the four-fermion final states and Z^0 hadronic decays was investigated yielding 13 and 20 events.

3   Simulated events

In order to evaluate the electron structure function one needs to measure two, independent variables, the polar angle θ_{tag} of the scattered (tagged) electron and its energy. Both these quantities are very well measured in the DELPHI experiment using the STIC luminometer. The effective θ_{tag} measurement in STIC ranges from $2.5°$ to $10°$ what at LEP-1 energies corresponds to a $|Q^2|$ interval starting effectively from 4.5 to 45 $(GeV/c)^2$. The squared-momentum Q^2 and the energy resolutions (that are $\frac{\sigma_{Q^2}}{Q^2} = 2.5\%$ and $\frac{\sigma_E}{E} = 2\%$ respectively), assure very precise measurement in the full range of considered variables. These directly measured quantities lead to an exact evaluation of z and Q^2 variables

describing the electron structure function (see formula (2)). In order to determine a detector response the measured cross-sections have been corrected using a detector efficiency, which is obtained on the basis of the comparison of a generated sample to a sample that passed the detector simulation program with the same reconstruction program as the experimental data. In general, the efficiency function is model dependent. Therefore it is very important to use an event-generator that descibes correctly the real data events. In this analysis TWOGAM event generator together with the JETSET Parton Shower algoritms for the quark and gluon fragmentation have been used. This generator tested for years with good results in DELPHI turned out to be a reliable tool to determine the correct detector efficiency. The TWOGAM cross-sections are expressed in terms of three independent components:

- soft-hadronic part described by the Generalized Vector Dominance Model

- point-like component, QPM

- resolved photon interaction, RPC

Since there is a freedom in choice of the photon structure function the GRVLO parametrization was adopted. More detailed description of TWOGAM package can be found [6]. It was established that such description guarantees the relatively good agreement of the simulated sample with the real data.

The selection criteria presented in sect.1, imposed on real data sample has also been used for the simulated sample. In that way one obtains two sets of distributions which can be compared. For instance visible cross-sections for real data of the: 1/scattered electron angle $\cos(\theta_{tag})$, 2/ the probing photon virtuality Q^2, 3/ the scattered electron energy E' and finally 4/ visible hadronic invariant mass W_{vis} are compared to those obtained from simulated sample at the same luminosity (see Fig. 2). All compared distributions show good agreement. Such above stated equalities confirm simultaneously good agreement between reconstructed (e.g. corrected by the corresponding efficiencies) real data cross-sections and those obtained from model (generated sample).

4 Determination of the Electron Structure Function

The ESF, a function of two variables z and Q^2, can be extracted from formula (2) and reads (one follows a usual practice to present structure function in a logarithmic scale of the z variable)

$$F_2^e(\xi, Q^2) = C \frac{Q^4}{(1 + (1 - y)^2)} \frac{d^2\sigma_{ee \to eX}}{d\xi dQ^2} \tag{8}$$

where $\xi = log_{10}(z)$ and C is a product of all constant factors.

The measured function $F_2^e(\xi, Q^2)^{meas}$ has to be corrected in each $\Delta\xi_i \Delta Q_k^2$ bin by the corresponding detector response function $E(\xi, Q^2)$, yielding reconstructed ESF $F_2^e(\xi, Q^2)^{rec}$,

$$F_2^e(\xi, Q^2)_{ik}^{rec} = F_2^e(\xi, Q^2)_{ik}^{meas} E(\xi, Q^2)_{ik} \tag{9}$$

where

$$E(\xi, Q^2)_{ik} = \frac{F_2^e(\xi, Q^2)_{ik}^{gen}}{F_2^e(\xi, Q^2)_{ik}^{sim}} \tag{10}$$

Such a procedure is quite justified since migration effect of events generated in any of the (z, Q^2) bins to neighbouring bins, after passing the detector simulation, is small. In Fig. 2 and Fig. 3 one can see a smearing caused by the detector for both, the standard photon x-variable Eq.(1) and z-variable Eq.(4), where events with single value of x=0.1 and z=0.01 have been generated and next passed through the detector simulation program. In opposition to the z distribution that shows typical narrow gaussian-type resolution, the x distribution is shifted to higher values and spread over the whole region of x. For that reason the x distributions have to be treated in a special way by means of an unfolding procedure. The one-dimensional unfolding requires a knowledge on theoretical shape of the photon-photon invariant mass distribution in order to convert W_{vis} into W_{rec}, whereas the determination of the ESF is not sensitive to that distribution.

Next, the Electron Structure Function is averaged over Q^2 in considered region of the photon virtuality leaving only the ξ dependence. In this analysis the ESF for three Q^2 intervals, $Q^2 \in (4.5, 30) \, GeV^2$, $Q^2 \in (4.5, 15) \, GeV^2$ and $Q^2 \in (15, 30) \, GeV^2$, has been plotted (Fig. 5-7) and displayed in Table 1. The lower value for $Q^2 = 4.5 \, GeV^2$ is a kinematical limit caused by a cut on minimum $\theta_{tag} = 2.5°$ angle of the tagged electron. One should stress that in the last two ξ-bins, (-2.0,-2.4) and (-2.4,-2.8), the kinematically available Q^2 intervals are $(4.5, 20) \, GeV^2$ and $(4.5, 8.0) \, GeV^2$ respectively, what has been taken into account.

Both, statistical and systematic uncertaintes contribute to the error bars displayed in Fig. 5-7 and Table 1. The statistical is dominated by an effect of the limited number of events in the real data sample after all selection cuts. Since the simulated sample was larger, the contribution from uncertaintes of the detector efficiency are much smaller. The systematic uncertainty has the following contributions which were added in quadrature to the statistical one:

- Uncertaintes due to the energy ($\frac{\sigma_E}{E} = 2\%$) and scattering angle ($\sigma_\theta = 0.05°$) of the tagged electron measurements. To estimate this effect one standard deviation of the energy resolution distribution has been added to the energy E_{tag} for each event, and one standard deviation has been subtracted from this value. The same was performed for the θ_{tag} variable. For each, out of four combinations of the angles and energies, the ESF has been determined. This source of systematics was evaluated as the maximum of the differences among the four $F_2^e(z, Q^2)_{ik}^{simul}$ values.

  The maximum value of all differences has been taken as a contribution to systematic uncertainty.

- Uncertainty due to binning variation. This has been estimated evaluating the ESF for three different bin widths.

It should be amphasised that on average about 50 percent of the total uncertainty originates from the systematic one. There is still possible to reduce the total error increasing number of data events (for instance with LEP2 data). Given any parametrization of the Photon Structure Function one can convert it into Electron Structure Function according to formula (6). In Fig. 5-7 set of the ESF corresponding to GRVLO,GRVHO,SAS and finally LAC1, photon parametrizations is superimposed on the data points. In addition to the above real photon structure parametrisation we also show the SaS virtual photon structure parametrisation, marked as SAS-INT. It has been integrated over the virtuality

of the probed photon P^2 according to Eq. (6) up to $P^2_{max} = 3 \ GeV^2$ equal to the anti-tag condition value.

Table 1: Results for measurement of the electron structure function

$Q^2[GeV^2]$	$\langle Q^2 \rangle$	$-log_10(z)$	F_2^e	σ_{stat}	σ_{system}
(4.5-30.)	12.0	0.0-0.4	0.0	$\pm$ 0.00	$^{+0.00}_{-0.00}$
		0.4-0.8	0.51	$\pm$ 0.11	$^{+0.44}_{-0.41}$
		0.8-1.2	3.04	$\pm$ 0.33	$^{+0.24}_{-0.32}$
		1.2-1.6	5.09	$\pm$ 0.32	$^{+0.20}_{-0.35}$
		1.6-2.0	6.53	$\pm$ 0.25	$^{+0.21}_{-0.24}$
		2.0-2.4	7.61	$\pm$ 0.17	$^{+0.31}_{-0.38}$
		2.4-2.8	6.50	$\pm$ 0.14	$^{+0.17}_{-0.22}$
		2.8-3.2	0.00	$\pm$ 0.00	$^{+0.00}_{-0.00}$
(4.5-15)	8.5	0.0-0.4	0.00	$\pm$ 0.00	$^{+0.00}_{-0.00}$
		0.4-0.8	0.18	$\pm$ 0.13	$^{+0.43}_{-0.44}$
		0.8-1.2	1.75	$\pm$ 0.38	$^{+0.25}_{-0.36}$
		1.2-1.6	3.61	$\pm$ 0.37	$^{+0.22}_{-0.23}$
		1.6-2.0	5.52	$\pm$ 0.29	$^{+0.19}_{-0.24}$
		2.0-2.4	7.10	$\pm$ 0.19	$^{+0.34}_{-0.41}$
		2.4-2.8	6.69	$\pm$ 0.16	$^{+0.15}_{-0.22}$
		2.8-3.2	0.00	$\pm$ 0.00	$^{+0.00}_{-0.00}$
(15-30)	21.5	0.0-0.4	0.00	$\pm$ 0.00	$^{+0.00}_{-0.00}$
		0.4-0.8	0.72	$\pm$ 0.17	$^{+0.48}_{-0.49}$
		0.8-1.2	3.91	$\pm$ 0.50	$^{+0.31}_{-0.48}$
		1.2-1.6	5.66	$\pm$ 0.49	$^{+0.29}_{-0.15}$
		1.6-2.0	7.93	$\pm$ 0.38	$^{+0.21}_{-0.29}$
		2.0-2.4	9.02	$\pm$ 0.25	$^{+0.43}_{-0.60}$
		2.4-2.8	0.03	$\pm$ 0.14	$^{+0.18}_{-0.25}$
		2.8-3.2	0.00	$\pm$ 0.00	$^{+0.00}_{-0.00}$

5 Conlusion

The hadronic part of the electron structure function has been measured for the first time. The proposed method is explicit and simpler as compared to the photon structure analysis - it does not use the unfolding procedure. It also allows to take the virtuality of the probed photon into account. In general the analysis shows consistency of both (electron and photon) approaches. It is demonstrated that the migration of events between z-bins (electron) is much smaller than between x-bins (photon). The statistical uncertainties are well understood since in each bin of the measured ESF they reflect a Poisson error whereas statistical uncertainties obtained from the unfolding procedure seem to be underestimated.

Out of all presented models the GRVLO, SaS and P^2-dependent SaS follow the data whereas GRVHO and LAC1 do not. It should be stressed that the inclusion of the photon virtuality is important - the difference between two SaS parametrisations (P^2-dependent and $P^2 = 0$) are of the same order as between SaS and GRVLO (both with $P^2 = 0$).

References

[1] E. Witten, Nucl. Phys. **B120**, 189 (1977);
C.H. Llewellyn-Smith, Phys. Lett. **79B**, 83 (1978);
R.J. DeWitt et al., Phys. Rev. **D19**, 2046 (1979);
T.F. Walsh and P. Zerwas, Phys. Lett. **36B**, 195 (1973); R.L. Kingsley, Nucl. Phys. **B 60**, 45 (1973).

[2] W. Słomiński and J. Szwed, Phys. Lett. **B387**, 861 (1996); Acta Phys. Polon. **B27** 1887 (1996); ibid **B28** 1493 (1997); ibid **B29** 1253 (1999). W. Słomiński, Acta Phys. Polon. **B30**, 369 (1999).

[3] W. Słomiński and J. Szwed, Eur. Phys. J. **C22**, 123 (2001);

[4] H.J. Behrend et al., CELLO Collaboration, Phys. Lett. **126B**, 391 (1983); Ch. Berger et al., PLUTO Collaboration, Phys. Lett. **142B**, 111 (1984); Nucl. Phys. **B281**, 365 (1987); W. Bartel et al., JADE Collaboration, Zeit. f. Phys. **C24**, 231 (1984); M. Althoff et al., TASSO Collaboration, Zeit. f. Phys. **C31**, 527 (1986); H. Aihara et al., TPC/2γ Collaboration, Zeit. f. Phys. **C34**, 1 (1987); Phys. Rev. Lett. **58**, 97 (1987); T. Sasaki et al., AMY Collaboration, Phys. Lett. **252B**, 491 (1990); R. Akers et al., OPAL Collaboration, Zeit. f. Phys. **C61**, 199 (1994); S.K. Sahu et al., AMY Collaboration, Phys. Lett. **B346**, 208 (1995); P. Abreu et al., DELPHI Collaboration, Zeit. f. Phys. **C69**,223 (1996); K. Ackerstaff et al., OPAL Collaboration, Zeit. f. Phys. **C74**, 33 (1997); Phys. Lett. **B411**, 387 (1997); ibid. **B412**, 225 (1997); M. Acciarri et al., L3 Collaboration, Phys. Lett. **B436**, 403 (1998); ibid. **B447**, 147 (1999; ALEPH Collaboration, Phys. Lett. **B458**, 152 (1999).

[5] DELPHI Collab., P.Aarnio et al., Nucl. Instr. and Methods., **A378**, 57 (1996)

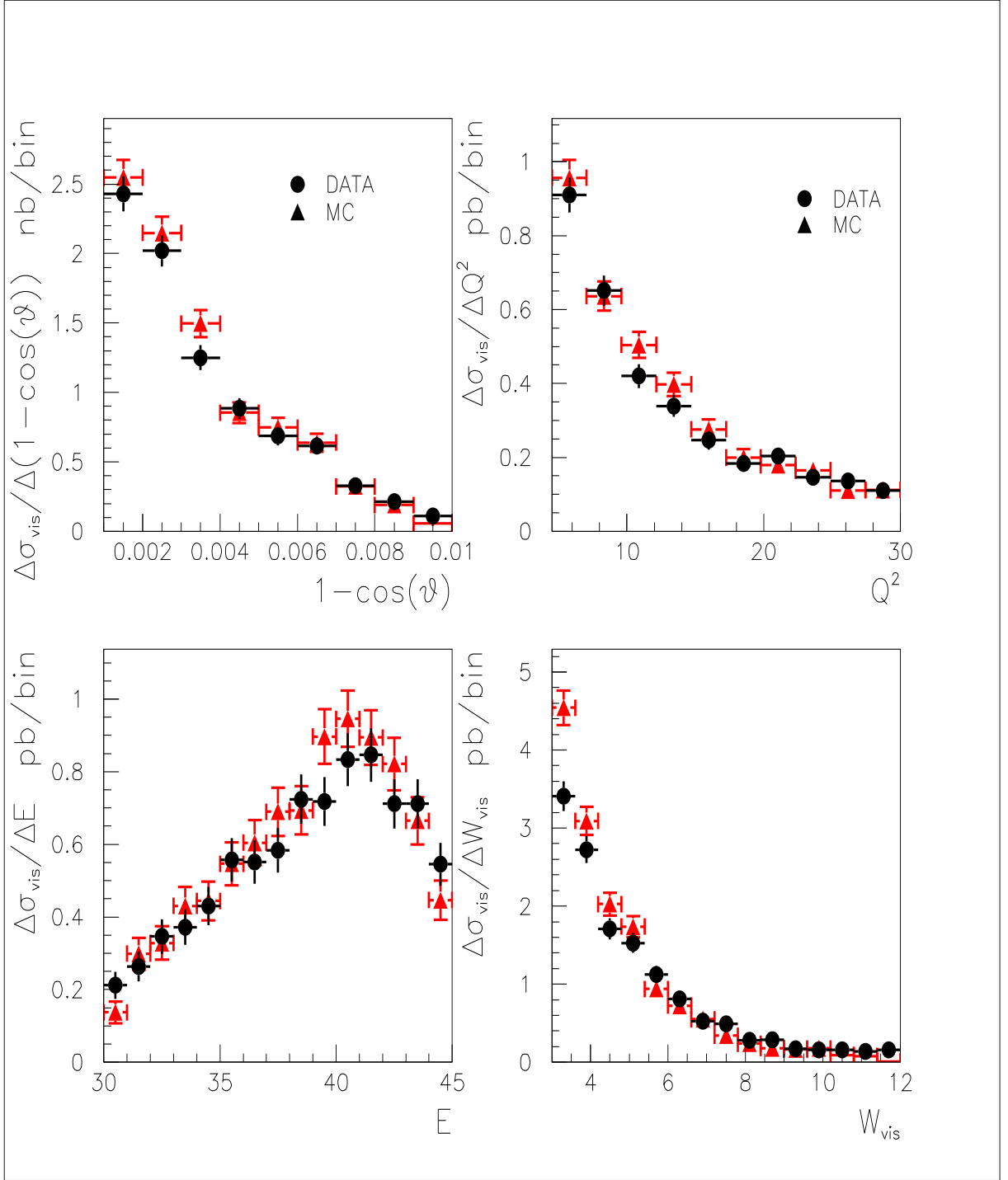[6] S. Nova, A. Olshevsky, T. Todorov, DELPHI-90-35 (unpublished).

Figure 2: The $\frac{\Delta\sigma_{vis}}{\Delta(1-cos(\theta))}$, $\frac{\Delta\sigma_{vis}}{\Delta Q^2}$ $\frac{\Delta\sigma_{vis}}{\Delta E_{tag}}$ and $\frac{\Delta\sigma_{vis}}{\Delta W}$ visible cross sections for real and simulated data
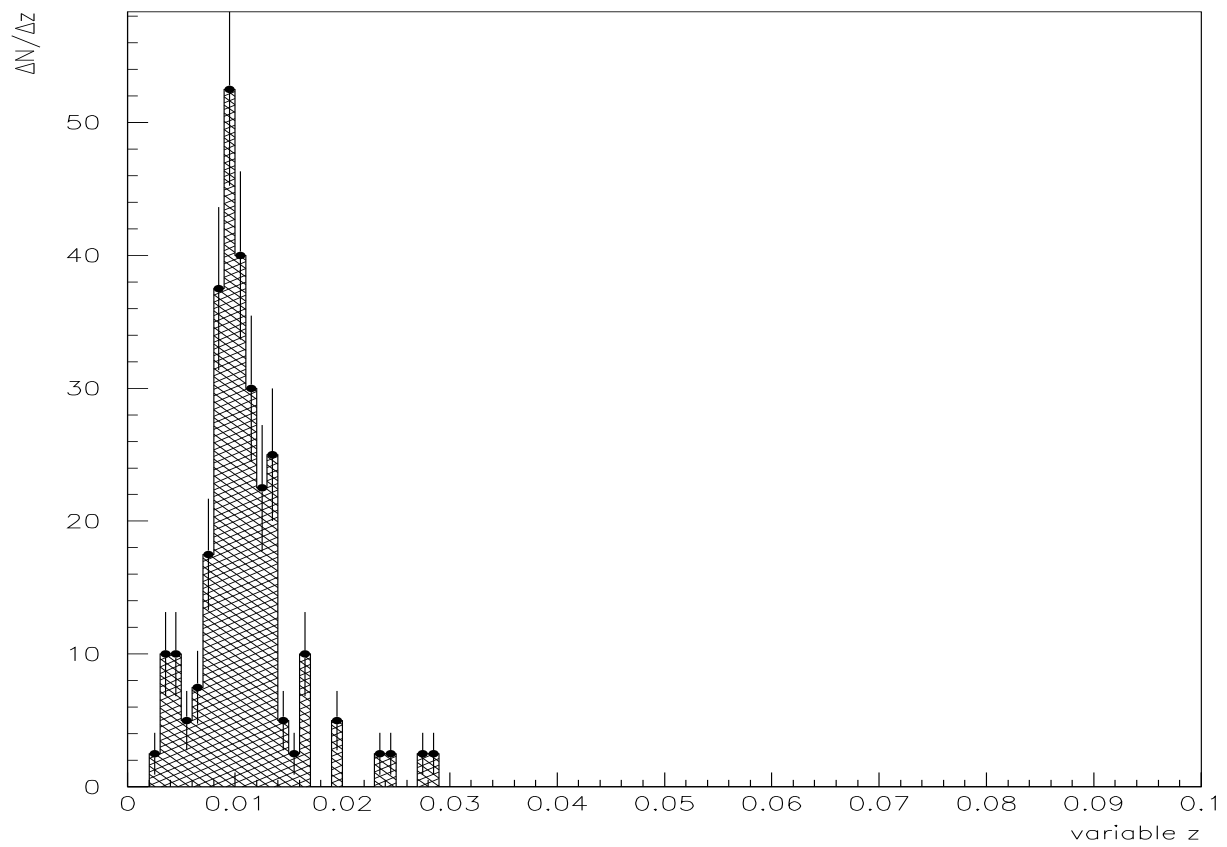
9

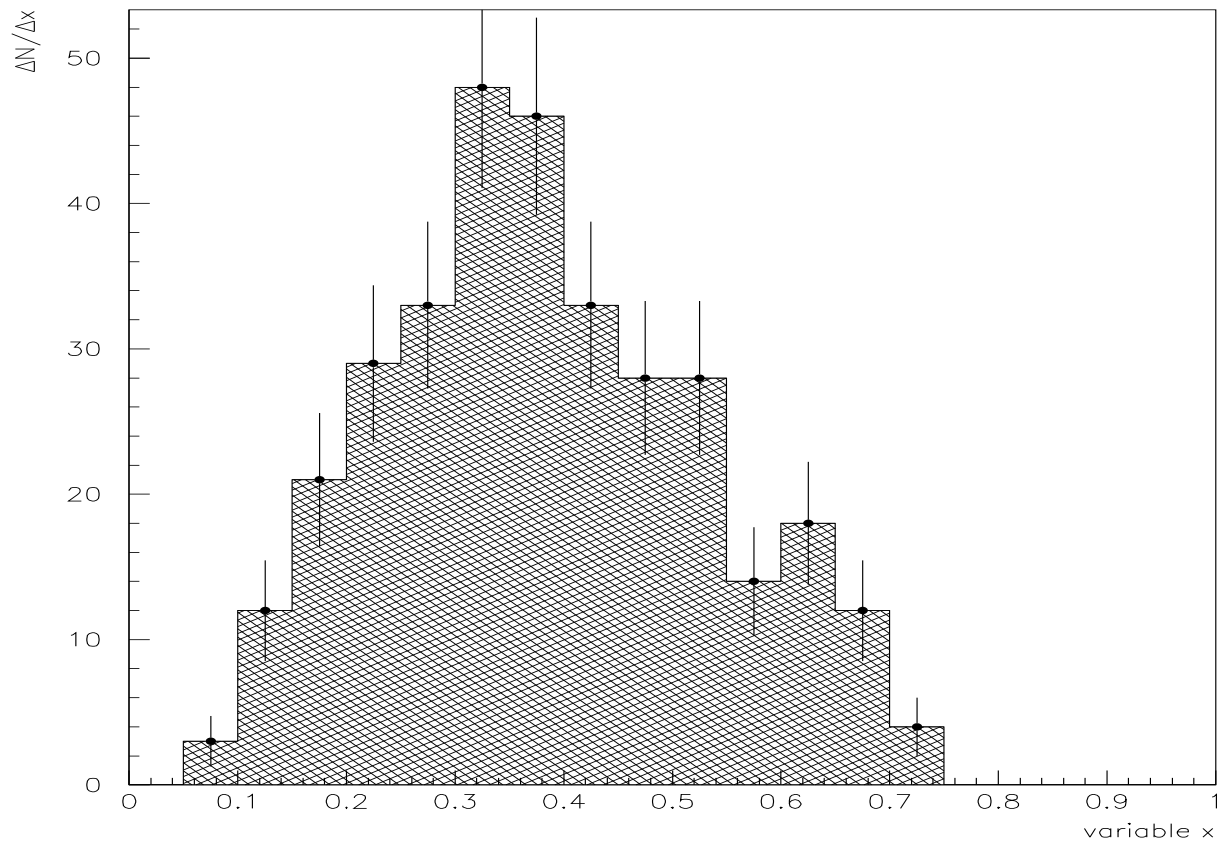Figure 3: The detector simulated z-distribution obtained from the sample generated at z=0.01

Figure 4: The detector simulated x-distribution obtained from the sample generated at x=0.1
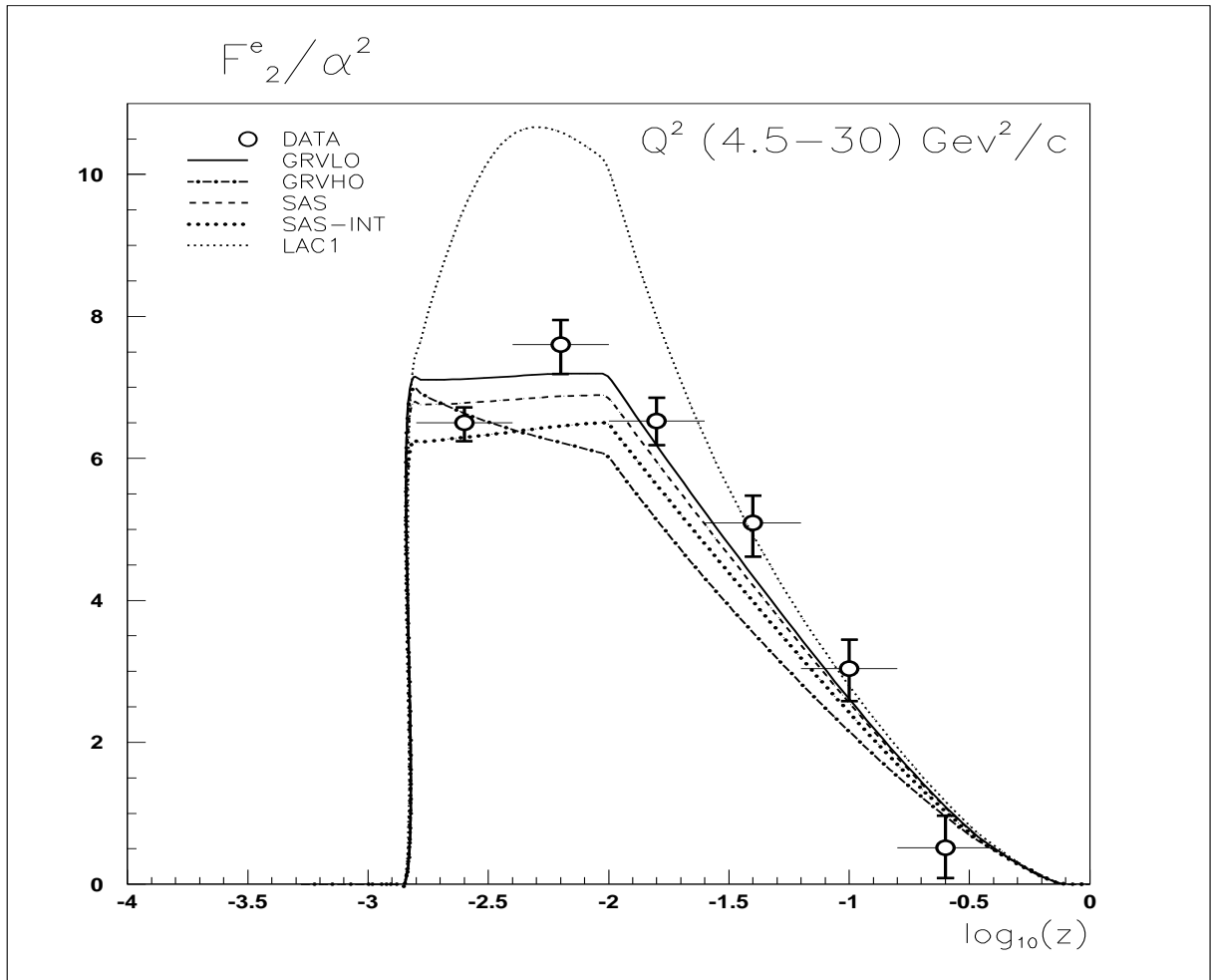
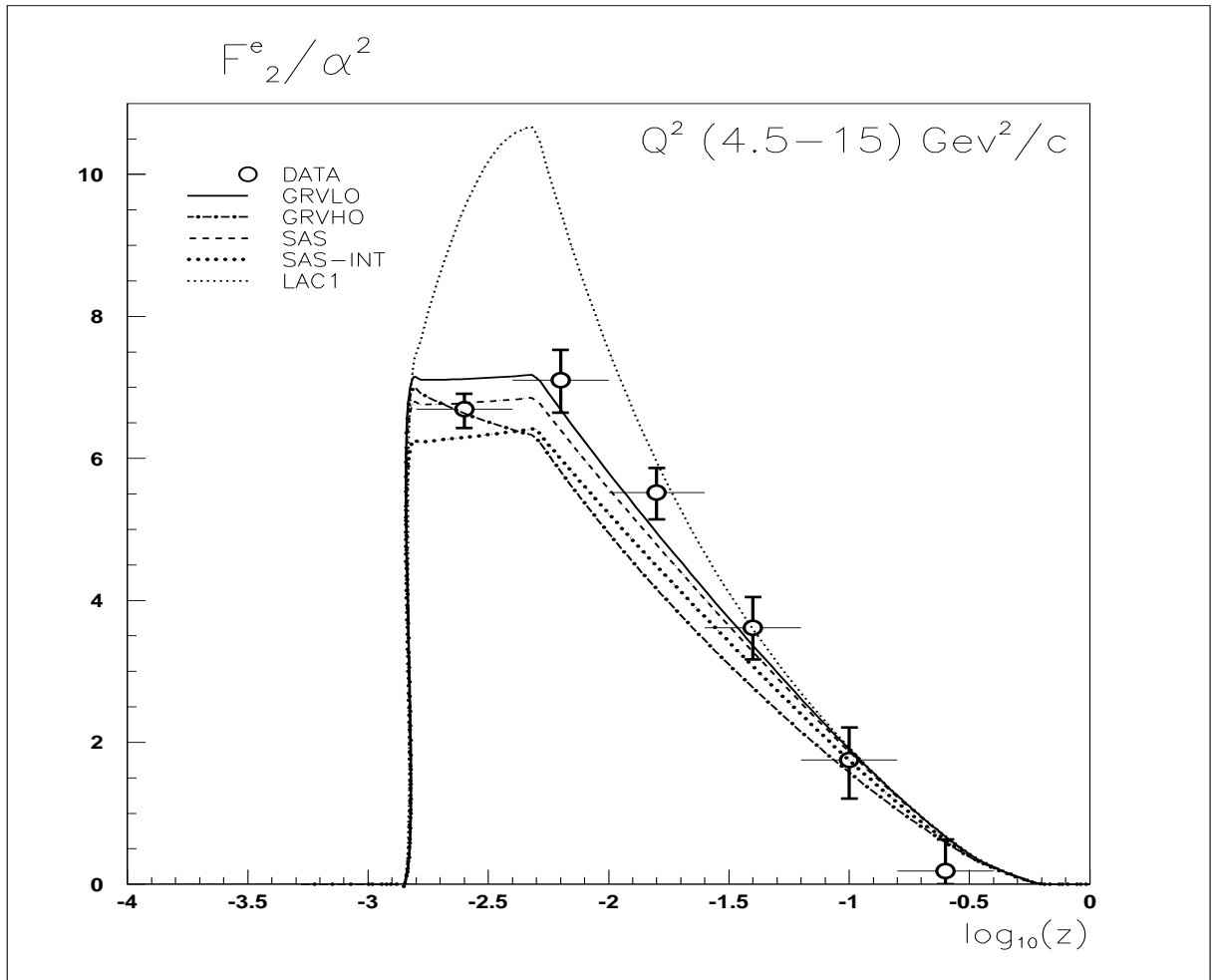Figure 5: The electron structure function averaged over $Q^2 \in (4.5, 30)\, GeV^2$ (see also text)

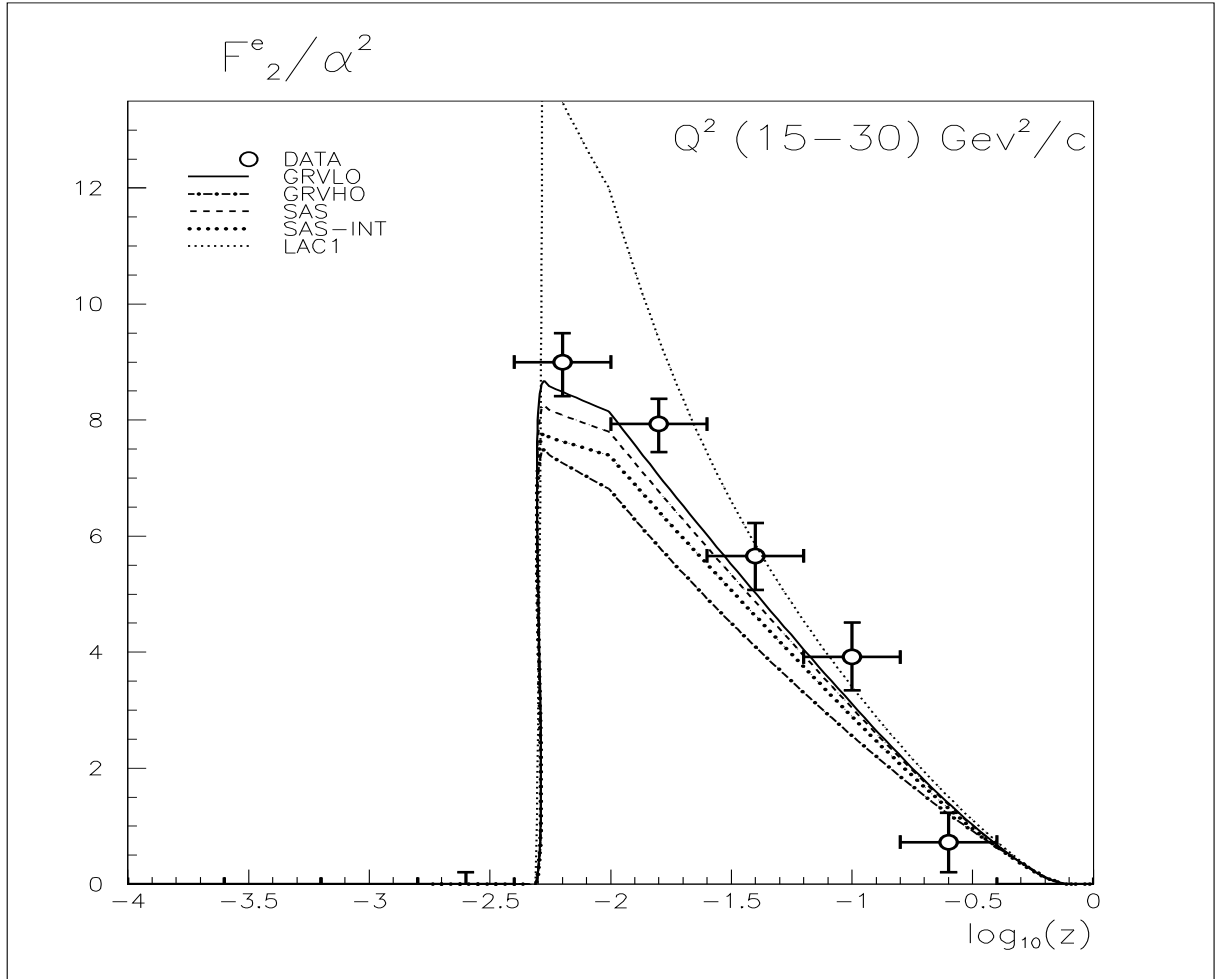Figure 6: The electron structure function averaged over $Q^2 \in (4.5, 15)\, GeV^2$ (see also text)

Figure 7: The electron structure function averaged over $Q^2 \in (15, 30) \, GeV^2$ (see also text)